Coda-derived source properties estimated using local earthquakes in the Sea of Marmara, Türkiye

Berkan Özkan[1], Tuna Eken[1], Peter Gaebler[2], Tuncay Taymaz[1]

[1] Department of Geophysical Engineering, Faculty of Mines, Istanbul Technical University, Maslak, 34467 Istanbul, Türkiye
[2] BGR Federal Institute for Geosciences and Natural Resources, Stilleweg 2, 30655, Hannover, Germany

Correspondence to: Berkan Özkan (ozkanber@itu.edu.tr)

Abstract. Accurate estimates of the moment magnitude of earthquakes that physically measures the earthquake source energy are crucial for improving our understanding of seismic hazard in regions prone to tectonic activity. To address this demand, a method involving coda wave modelling was employed to estimate the moment magnitudes of earthquakes in the Sea of Marmara, the north-western Türkiye. This approach enabled us to model the source displacement spectrum of 303 local earthquakes efficiently recorded at 49 regional seismic stations between 2018 and 2020 in the region. The coda wave traces of individual events were inverted across twelve frequency ranges between 0.3 and 16 Hz. The resultant coda-derived moment magnitudes were found to be in good accordance with the conventional local magnitude estimates. However, the notable move-out between local magnitude and coda-derived moment magnitude estimates for smaller earthquakes less than a magnitude of 3.5 likely occurs due to potential biases arising from incorrect assumptions for anelastic attenuation and/or the finite sampling intervals of seismic recordings. Scaling relations between the total radiated energy and seismic moment imply a nonself-similar behaviour for the earthquakes in the Sea of Marmara. Our findings suggest that larger earthquakes in the study area exhibit distinct rupture dynamics compared to smaller ones, resulting in a more efficient release of seismic energy. Hence, here we introduce an empirical relationship obtained from the scatter between local magnitude and coda-derived moment magnitude estimates.

1 Introduction

Having a strong and consistent understanding of source properties (e.g., moment magnitude M_L, released energy E_R, seismic moment M_0) is extremely important in tectonically active regions such as the Sea of Marmara located at the northwest of the North Anatolian Fault Zone (NAFZ) in NW Türkiye. This is essential for accurately assessing seismic hazard potential, as it primarily relies on creating dependable seismicity catalogues. Likewise, precise data on source parameters plays a significant role in the development of regional attenuation properties.

Traditional magnitude scales such as local, body wave, or surface wave magnitude scales (M_L, m_b, M_S) derived from direct wave analyses may exhibit bias due to diverse factors including source radiation pattern, directivity, and path heterogeneities. These effects can cause significant changes in direct wave amplitude measurements (e.g., Favreau and Archuleta, 2003). Over

the past four decades since pioneering study of Aki (1969), computational seismology has achieved remarkable progress, enabling the integration of scattered wavefields, i.e., coda waves, into studies of source parameters (e.g., Sato et al., 2012). These developments have expanded our understanding of seismic events and improved the accuracy of source parameter estimation. Aki and Chouet, (1975) spotted that these scattered wave train and its spectral content behave similarly at recordings of different stations for a given earthquake. They further noticed coda duration is independent of azimuth or epicentral distance. More recently, studies analysing local and/or regional coda envelopes suggest that coda wave amplitudes are notably less variable, about 3 to 5 times, compared to direct wave amplitudes (e.g., Mayeda and Walter, 1996; Mayeda et al., 2003; Eken et al., 2004; Malagnini et al., 2004; Gök et al., 2016). It is widely recognized that local or regional coda waves mainly consist of scattered waves. These wave trains can be explained by Aki's single-scattering model (1969), which is significantly less sensitive to source radiation pattern effects compared to direct waves, owing to the volume-averaging property of coda waves that sample entire focal sphere (e.g., Aki and Chouet, 1975; Rautian and Khalturin, 1978). For a more in-depth understanding of coda generation theory and advances in empirical observations and modelling efforts, have been analysed and summarised in Sato et al. (2012).

Various methods depending on coda waves analysis have been utilized for earthquake source scaling. They are usually categorized into two groups. The first group of methods is known as the parametric approach and involves employing a coda normalization strategy. This requires applying corrections (including path effect, S-to-Coda transfer function, site effect, and any distance-dependent changes in coda envelope shape) on the measurements extracted from coda wave envelopes through empirically derived quality factors that account for seismic attenuation parameters (e.g., intrinsic and scattering factors) or site effect caused by near surface geology conditions. To determine the final source properties, reference events with pre-estimated seismic moments based on waveform inversion techniques are used. Forward calculation of the synthetic coda envelopes is achieved by using either single-backscattering or more advanced multiple-backscattering approximations (Sato et al., 2012). Empirical coda envelope methods have been successfully applied in regions with complex tectonics, such as northern Italy (e.g., Morasca et al., 2008), throughout Türkiye and the Middle East (e.g., Mayeda et al., 2003; Eken et al., 2004; Gök et al., 2016), and the Korean Peninsula (e.g., Yoo et al., 2011).

The approaches in the second group involve estimating source and structural properties using a joint inversion technique in which source-, path-, and site-specific factors are optimized simultaneously by comparing observed coda envelope with its physically derived representative synthetic coda envelope within a selected time window including both the observed coda and direct S-wave parts. While the conventional coda normalization method corrects for undesired effects of source and site amplifications, it may not work well for small events with short coda lengths. This occurs mainly due to dominating random seismic noise that disrupts the requirement of a homogeneous coda wave energy distribution in space. To overcome this limitation, we incorporate source excitation and site amplification terms in the inversion process in which synthetic coda wave envelopes are analytically expressed via the radiative transfer theory (RTT). The RTT was originally implemented on coda waves by Sens-Schönfelder and Wegler (2006), and has been successfully tested on local and regional earthquakes ($4 \leq M_L \leq 6$) detected by the German Regional Seismic Network. Moreover, it has been applied to investigate source- and frequency-

dependent attenuation properties in various geological settings, including the upper Rhine Graben and Molasse basin regions in Germany (Eulenfeld and Wegler, 2016), western Bohemia–Vogtland in Czechia (Gaebler et al., 2015a), the entire United States (Eulenfeld and Wegler, 2017), and the central and western NAFZ (Gaebler et al., 2019; Izgi et al., 2020). Previous studies (Gusev and Abubakirov, 1996) have further considered a more realistic Earth model with anisotropic scattering conditions, resulting in peak broadening effects of direct seismic wave arrivals. The propagation of P-wave elastic energy and the conversion between P- and S-wave energies with this approach has been used in Zeng et al. (1991), Przybilla and Korn (2008), and Gaebler et al. (2015b).

In this study, we generate source spectra for 303 local events with magnitudes $2.5 \leq M_L \leq 5.7$ that occurred in the Sea of Marmara region as the product of a joint inversion of S-wave and coda wave components extracted. To estimate coda-derived source spectra and further moment magnitude and total radiated seismic energy of these selected earthquakes we utilized an open-source python based Qopen software (Eulenfeld, 2020), which employs the isotropic acoustic RTT to calculate synthetic coda envelopes. Gaebler et al. (2015a) have noted that modelling outcomes from isotropic scattering were nearly equivalent to those inferred from more complex elastic RTT simulations with anisotropic scattering conditions. Adopting the joint inversion technique offers advantages, as it remains unaffected by potential biases that could arise from external information, such as i.e., source properties of a reference earthquake that are separately estimated and then used for calibration in coda-normalization methods. The advantage of the approach exploited in this work stems from the analytical expression of a physical model incorporating source- and path-related parameters to describe the scattering process. Furthermore, the optimization process during the joint inversion enables source parameter estimates for relatively small-size events compared to those employed in coda normalization methods.

2 Regional Settings and Seismic Hazard Potential in the Sea of Marmara, NW Türkiye

Our study area is the Sea of Marmara, located in the northwest of the 1600-km-long right lateral strike-slip North Anatolian Fault Zone (NAFZ) that outlines a boundary between the Eurasian plate to the north and the Anatolian plate to the south (Taymaz et al., 1991, 2004, 2007, 2021). The NAFZ has experienced numerous devastating historical earthquakes that have ruptured throughout its the entire length with an overall westward migrating pattern (Stein et al., 1997). The first major earthquake of significant consequence within our specific area of interest occurred along the Ganos segment situated at the westernmost part of the NAFZ in 1912. More recently, two destructive earthquakes, namely the Izmit earthquake (M_w 7.4, August 17, 1999) and the Düzce earthquake (M_w 7.2, November 12, 1999), have affected the north-western branch of the NAFZ. Barka et al. (2002), depending on the historical earthquake records published in Ambraseys and Jackson (2000) has reported the region lying between the 1912 and 1999 ruptures represents a seismic gap in the Sea of Marmara. Following the 1999 M_w 7.4 Izmit earthquake, Coulomb stress change calculations performed by King et al. (2001) and Durand et al. (2013) demonstrate that new stress accumulation is focused on this western branch in the Sea of Marmara. In fact, precise locations of microseismicity indicated that the two 1999 earthquakes activated seismicity to the south of Istanbul along the northwest

branch of the NAFZ beneath the Sea of Marmara (e.g., Bohnhoff et al., 2013; Sato et al., 2004; Schmittbuhl et al., 2016). Martínez-Garzón et al. (2019, 2022) have indicated that a frequent interaction between seismic and aseismic slip based on their analyses on microseismicity recordings and borehole strainmeter data from the eastern Marmara. The seismic gap along the northern segment of the NAFZ within the Çınarcık Basin at the eastern shear zone of the Sea of Marmara is well identified by high-resolution observations of microseismicity (e.g., Sato et al., 2004; Bohnhoff et al. 2013) and geodetic locking depth estimates (Ergintav et al., 2014). The existing seismic gap of ~150 km unruptured Main Marmara Fault segment (the combination of North Boundary and Central Marmara segment) of the NAFZ beneath the Sea of Marmara has been subject to several studies mainly involving spatio-temporal microseismicity characteristics (e.g., Sato et al., 2004; Bohnhoff et al., 2013; Schmittbuhl et al., 2016; Wollin et al., 2018; Irmak et al., 2021). This area is predicted to be the location of a potential major earthquake in the future, postulated by Bohnhoff et al. (2013). Therefore, it is crucial to have accurate estimates of the physical measures of energy released during small-to-moderate size earthquakes to improve seismic hazard assessments in this tectonically active region.

3 Data

In this study, we exploited digital waveforms of local earthquake recordings from at 49 broadband seismic stations in the Sea of Marmara between 2018 and 2020 (Fig 1). We benefited from revised earthquake catalogue information acquired from the Kandilli Observatory and Earthquake Research Institute (KOERI) to extract waveform data for a total of 375 examined events with station–event pair distance less than 200 km and focal depths less than 20 km. The majority of seismic activity related to NAFZ in the Sea of Marmara. There are no further requirements, such as taking geographical distribution or azimuthal coverage into account as coda waves provide a path-wide averaging effect (e.g., Mayeda et al., 2003).

Here, to start with we first deconvolve the instrument response to better mimic the actual ground motion on seismograms. Our data pre-processing steps involved band-pass filtering of velocity seismograms using a Butterworth type band-pass filter at several frequency bands with central frequencies of 0.3, 0.5, 0.7, 1, 1.4, 2.0, 2.8, 4.0, 6.0, 8.0, 12.0, 16.0 Hz that varied depending on the spectral content of a specified event.

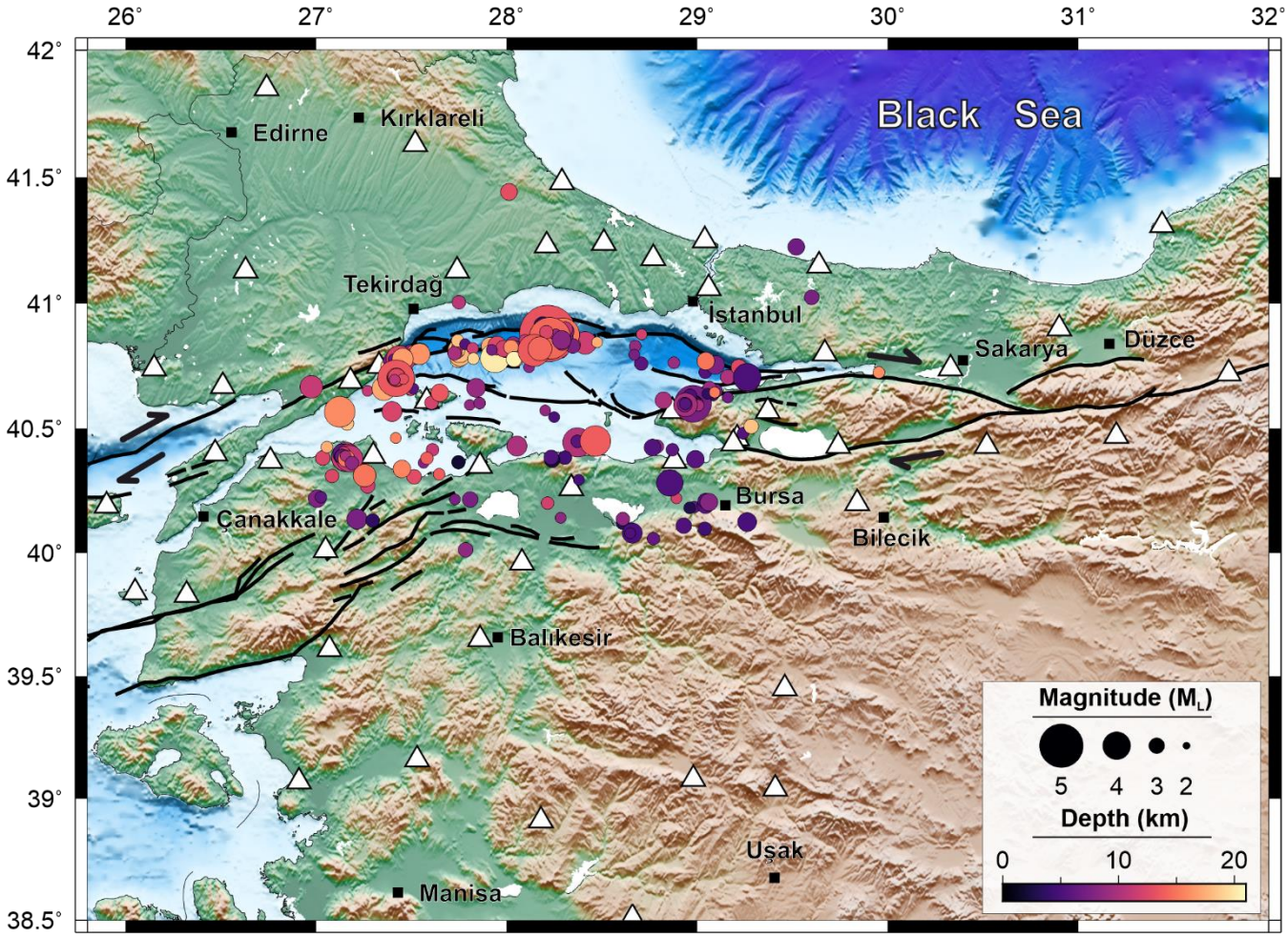

Figure 1: Spatial distribution of 303 local events ($2.5 \leq M_L \leq 5.7$) occurred between 2018 and 2020 are displayed with circles color-coded by focal depths reported by the KOERI catalogue. White triangles indicate used stations in the present work.

Later, we performed a Hilbert transform on the filtered waveform data between each frequency bands to generate the total energy envelopes. To predict the P- and S-wave onsets on these envelopes, an average crustal velocity model was employed. Based on this information, several steps taken to ensure to more accurate M_0, and thus coda-derived moment magnitude (M_{w-coda}) can be given as follows:

i. The noise level before the P-wave onset was disregarded,

ii. The S-wave window was defined, starting 8 s prior to and 10 s after the S-wave onset to include all direct S-wave energy effectively,

iii. Following the S-wave window, a coda window starts at 5 s before and ends 150 s after the S-wave onset or it ends if signal-to-noise ratio (SNR) of 3.

Here it is worth mentioning that the length of the coda windows might be shortened under two circumstances: when the SNR is less than 2.5, or when coda waves from two earthquakes (e.g., aftershock sequences) occur within the same analysis window, leading to an additional rise rather than a decrease in the envelope.

The earthquakes with less than 10 s of coda length and the earthquakes with the recordings of less than 4 stations were disregarded by our automated process. We further conducted a visual inspection on each waveform to assure high-quality data. After applying these criteria, 6557 station-event pairs from 303 out of 375 all analysed earthquakes ($2.5 \leq M_L \leq 5.7$ within a radius of 200 km) remained for further data modelling process.

4 Method

4.1 M_{w-coda} Estimation

We used an inversion scheme adopted by Eken (2019). Procedure was originally developed by Sens-Schönfelder and Wegler (2006), and later on Eulenfeld and Wegler (2016) modified it to model intrinsic and scattering attenuation parameters.

The forward part dealing with the energy density computation for a particular frequency band assuming a source that emits radiation uniformly in all directions (isotropic), is given by Sens-Schönfelder and Wegler (2006) as follows,

$$E_{mod}(t,r) = WR(r)G(t,r,g)e^{-bt} \tag{1}$$

where R and W indicate the energy site amplification factor, and source term, respectively. b represents the intrinsic attenuation parameter. $G(t,r,g)$ indicates the Green's function and considers both direct and scattered wave fields. Its analytical expression is given by Paasschens (1997) as follow:

$$G(t,r,g_0) = \exp(-v_0 t g_0)\left[\frac{\delta(r-v_0 t)}{4\pi r^2} + \left(\frac{4\pi v_0}{3g_0}\right)^{-\frac{3}{2}} t^{-\frac{3}{2}}\left(1-\frac{r^2}{v_0^2 t^2}\right)^{\frac{1}{8}} K\left(v_0 t g_0\left(1-\frac{r^2}{v_0^2 t^2}\right)^{\frac{3}{4}}\right) H(v_0 t - r)\right] \tag{2}$$

with $K(x) = e^x\sqrt{1+\frac{2.026}{x}}$

where g_0 is the scattering coefficient and v_0 is the mean S-wave velocity. In Eq. 2 the term given within the Dirac delta function describes the direct wave and the rest represents scattered wave part of the Green's function.

Potential differences between predicted and observed energy densities for each earthquake recorded at each station using N_{ij} time samples in a specific frequency band can be minimized by

$$\epsilon(g) = \sum_{i,j,k}^{N_S,N_E,N_{ij}}\left(\ln E_{ijk}^{obs} - \ln E_{ijk}^{mod}(g)\right)^2 \tag{3}$$

where, N_S and N_E represent the numbers of stations (index *i*) and events (index *j*), respectively. Then the scattering attenuation parameter (g) will be optimized following Eq. 4.

$$\ln E_{ijk}^{obs} = \ln E_{ijk}^{mod}(g) \quad (4)$$

Substituting Eq. 1 into Eq. 4 will give Eq. 5

$$\ln E_{ijk}^{obs} = \ln G\left(t_{i,j,k}, r_{ij}, g\right) + \ln R_i + \ln W_j + bt_{ijk} \quad (5)$$

Eq. 5 contains $\sum_{i,j} N_{ij}$ equations and $N_S + N_E + 1$ variables as it indicates an overdetermined inversion problem by having b, R_i, and W_j unknown parameters. Thus Eq. 5 can be solved by using a least-squares approach. $\epsilon(g)$ can be defined by the sum over the squared residuals of the solution.

The three main steps followed in this inversion scheme to optimize unknown model parameters (g, b, R_i, and W_j) are given in Eulenfeld and Wegler (2016).

i. Calculation of the Green's function for fixed scattering parameter g and minimizing Eq. 5 to solve for b, R_i, and W_j.
ii. Calculation of ϵ(g) through Eq. 3.
iii. Repeating the step i and ii by letting g to vary to find the optimal b, R_i, and W_j, until the error function ϵ(g) is minimized.

In Fig. 2 we present an example for this minimization process that was applied to the observed coda envelopes at twelve different frequency bands generated by using one selected earthquake recorded at 49 seismic stations of the study area.

The yield of the minimization of the error function ϵ(g) outlined above will be the spectral source energy term W_j, site response R_i, and attenuation parameters b and g, that satisfy the optimal fitting between observed and predicted coda envelopes.

Using spectral source energy W in frequency domain, source displacement spectrum and thus M_0 and M_w can be obtained. (Sato et al., 2012) describe the S-wave source displacement spectrum considering a double-couple source in the far field as,

$$\omega M(f) = \sqrt{\frac{5\rho_0 v_0^5 W}{2\pi f^2}} \quad (6)$$

Here W is the radiated S-wave energy at a center frequency f, v_0 is the mean S-wave speed, and ρ_0 is the density of the medium.

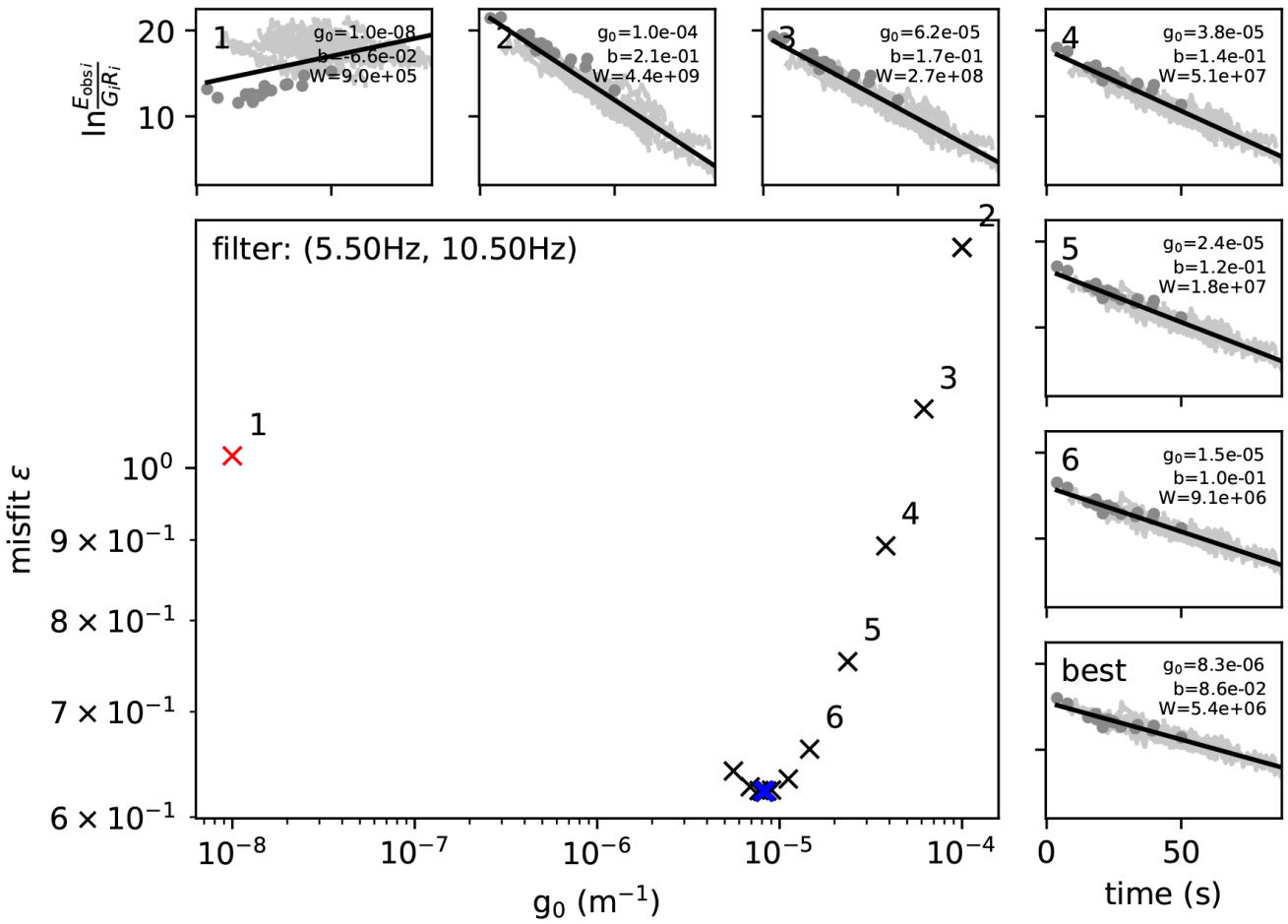

Figure 2: Optimization process for the event (30 November 2018 $M_L = 2.9$ and $M_{w-coda} = 3.02$) recorded at 23 diverse stations (frequency band 5.5 Hz - 10.5 Hz). Large panel shows the plot of the ϵ as a function of g_0 for the given frequency band. Blue cross shows the least misfit. Numbered small panels display least square solutions for the different g_0 guesses and best fit for optimal g_0. Dark grey dots represent the ratio E_{obs}/GR and grey lines represents the observed envelopes from different stations. Thick black line is the line-fit to estimate b and W by using its slope.

Abercrombie (1995) elucidated the correlation between the obtained source displacement spectrum and the M_0 by

$$\omega M(f) = M_0 \left(1 + \left(\frac{f}{f_c}\right)^{\gamma n}\right)^{-\frac{1}{\gamma}} \quad (7)$$

where n and γ represent the high frequency fall-off and the shape parameter, respectively. The latter determines the sharpness of the spectrum between the low-frequency constant level M_0 and the high-frequency fall-off with f^{-n}. By taking the natural logarithm of Eq. 7 we get then,

$$\ln \omega M(f) = \ln M_0 - \frac{1}{\gamma} \ln \left(1 + \left(\frac{f}{f_c}\right)^{\gamma n}\right) \quad (8)$$

The observed source displacement spectrum data $\omega M(f)$, can be used to determine the other parameters such as M_0, γ, n and f_c, in an inversion. Lastly, one of the aims of the present work can be done, M_{w-coda} can be derived from computed M_0, using the formula given by Hanks and Kanamori (1979):

In Eq. 8 essentially an optimization problem is outlined where the obtained data source displacement spectrum data (on the left) can be modelled to estimate four unknown parameters of the source (M_0, γ, n, and f_c). This is accomplished through a simultaneous least-squares inversion approach. Subsequently, M_{w-coda}, can be computed using the modeled source parameters and M_0, employing a formula introduced by Hanks and Kanamori (1979):

$$M_{w-coda} = \frac{2}{3}\log_{10} M_0 - 6.07 \quad (9)$$

4.2 Total Radiated Seismic Energy Estimation

In order to estimate the E_R first we integrate source displacement spectrum, $\omega M(f)$, and following the theoretical formula given by Gök et al. (2009). To be able to exploit the considerable part of the energy associated to the lower frequency part, observed spectrum is extrapolated to $f = 0\ Hz$.

Here the S-wave radiated energy (E_β) can be calculated by taking integral of the energy flux in a source sphere (Patton and Walter, 1993).

$$E_\beta = \frac{4\pi}{4\rho\beta^5}\int_0^\infty |M(f)|^2 df = \frac{\pi^2 f_c^3 M_0^2}{5\rho\beta^5} \quad (10)$$

where density $\rho = 2700\ kg/m^3$, s-wave velocity $\beta = 3.5\ km/s$. f_c and M_0 represent corner frequency and seismic moment estimates obtained from the inversion procedure described in Eq. 8. Here we assume that the contribution from the P-wave radiated energy (E_α) to the total radiated energy is about 7 % of S-wave (e.g., Boatwright and Fletcher, 1984; Mayeda and Walter, 1996). Finally, the sum of P-wave and S-wave radiated energies yield total seismic radiated energy (E_R).

5 Results and Interpretations

5.1 Coda Wave Envelope Fits

Our preferred acoustic RTT approach to perform forward calculation of the synthetic envelope modelling enabled the modelling of the S-wave energy propagation, thus the comparison between the synthetic and observed data, which is the portion of the seismograms directly between the S-wave arrival and the subsequent seismic coda. Previously Ryzhik et al. (1996) and Gaebler et al. (2015b) proved the validity of this approach due to the dominance of S-wave energy throughout the seismic signal, encompassing both the initial S-wave arrival and the later portions of the seismic coda. In Fig. 3, envelope fit results are presented for a selected earthquake with M_L 2.9 at different frequency bands (with central frequencies of 3.0, 4.0, 6.0, 8.0, 12.0 and 16.0). The data windows length of coda wave trains ranged from -10 s to 100 s relative to the onset time for

all events in the present study. For the optimization process, the bounds for g_0 and b were chosen to vary between $10^{-8} - 10^{-4}$ and $10^{-3} - 10^{1}$, respectively. Ultimately, unknown g_0, b, and W is determined by selecting the most suitable combination of model parameters enabling the lowest error value within each frequency band. Figure 2 shows a summary of inversion process behind the envelope fitting process. Accordingly, we can understand the range of the tested g0 values and further associated estimations of b and W at each iteration. Overall coda envelope fittings clearly illustrates that the synthetic coda envelopes are effectively required by the observed data across diverse regions within the study area and for events with varying magnitudes. The decay of the seismic coda within time windows of up to -10 - 100 seconds is also precisely modelled, with a notable faster decay for higher frequencies. The quality of the envelope fits is comparable to those previously presented by Gaebler et al. (2015a), Eulenfeld and Wegler (2016), Gaebler et al. (2019), Eken (2019), and Izgi et al. (2020).

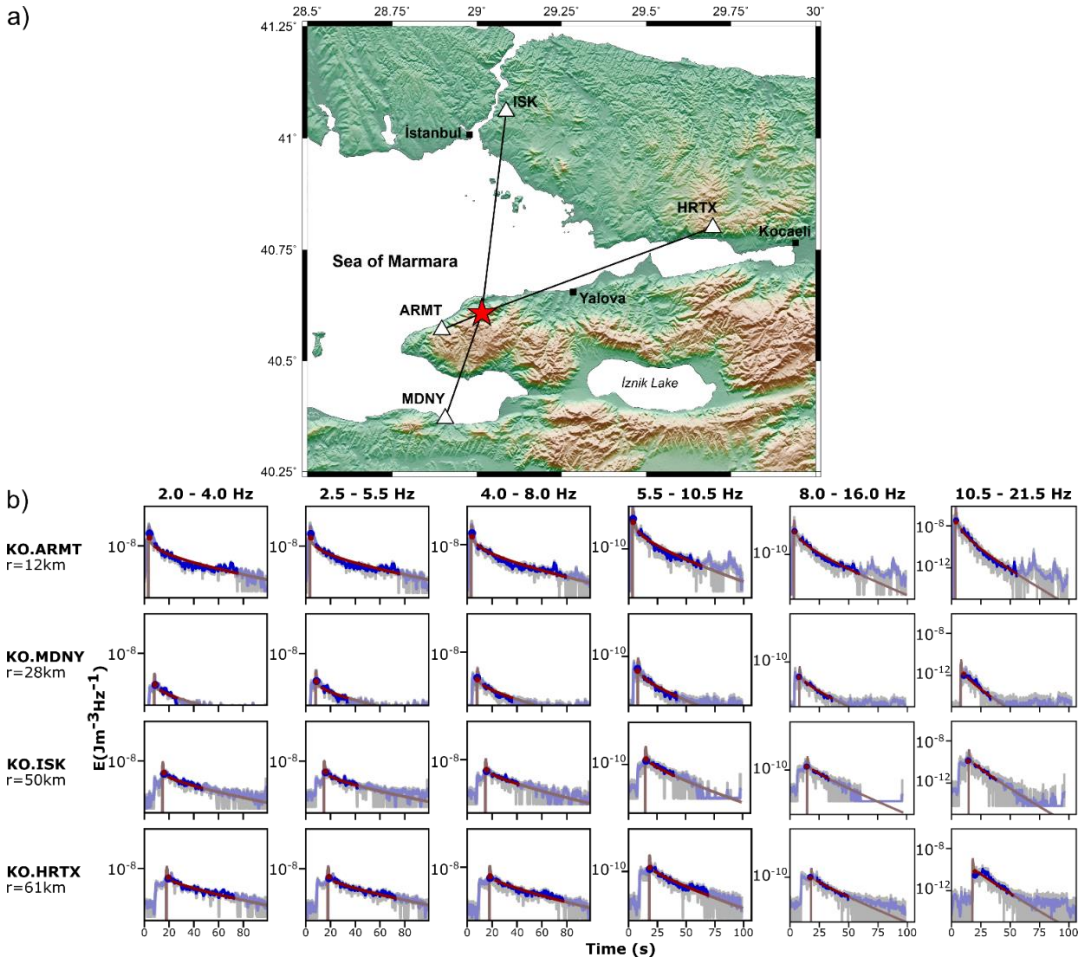

Figure 3: a) Example event occurred in 30 November 2018 with $M_L = 2.9$ (shown with red star) and station pairs (shown with white triangles). b) Fits between observed and calculated energy densities for an example event. Grey and blue lines indicate the observed and its smoothed version, respectively. Red curves represent the computed synthetic envelopes calculated using the inversion process.

5.2 Coda Wave Source Spectra

We present the observed values of 303 source spectra (Fig. 4) that were generated by implementing estimated spectral source energy term W at each frequency into Eq. 7. In overall, the obtained spectra models (Fig. 4) appear to be well consistent with a typically expected shape of a source displacement spectrum, featuring a flat region at around the low-frequency limit and a gradual decrease beyond a corner frequency. Earlier Walter et al. (1995) and Mayeda et al. (2003) have shown the use of coda waves would be more advantageous in scaling-up the earthquake size as they are rather insensitive to differences in the source radiation pattern and path effect. This mainly stems from the influence of multiple-scattering caused by small-scale heterogeneities lead to an averaging effect on coda waves. Eulenfeld and Wegler (2016) claimed the minor impact of radiation pattern on S-wave coda, but that it could potentially disrupt attenuation models inferred from direct S-wave analyses if the station distribution concerning the earthquakes lacks comprehensive azimuthal coverage. The characteristics of a source displacement spectrum, for example, f_c, M_0, and n may be misleading in traditional approaches (e.g., Abercrombie, 1995; Kwiatek et al., 2011) as they often underestimate potential complexities of the source and structure by considering a fixed frequency-independent attenuation effect described by a factor exponent ($-\pi f t Q^{-1}$) over the spectrum and an omega-square model (Brune, 1970) with a constant high-frequency fall-off parameter, $n = 2$. In the present work, however, we build the source spectra based on a source term decomposed from the effect of intrinsic and scattering attenuation. Separate estimation of source and structure-related terms is achieved by a simultaneous inversion procedure in which the high-frequency fall-off parameter changes. In line with previous investigations (e.g., Ambeh and Fairhead, 1991; Eulenfeld and Wegler, 2016), we also noted that adopting a more realistic methodology, as opposed to the traditional approach using the omega-square model (where $n > 3$), led to notable discrepancies. These deviations are significant to prompt a reassessment of the widely accepted use of this model for explaining minor earthquakes.

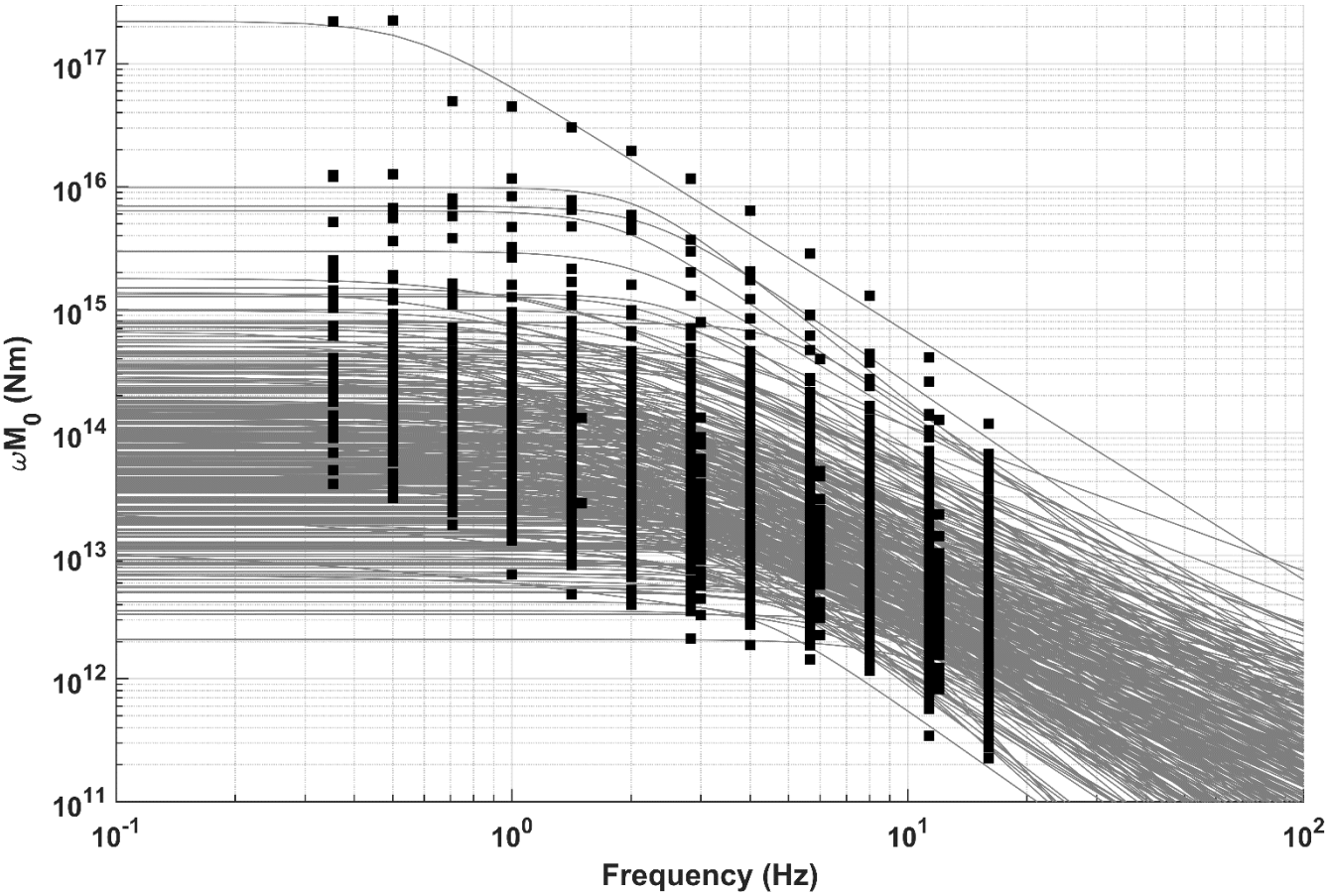

Figure 4: Black squares indicate observed source displacement spectra and grey curves represents predicted source displacements spectra for all individual 303 local earthquakes.

Earlier observations (e.g., Papageorgiou and Aki, 1983; Atkinson, 1990; Joyner, 1984) indicated that source spectra, especially for large earthquakes, could be better described by models involving two corner frequencies. More recently, Denolle and Shearer (2016) reported that the conventional single-corner frequency spectral model failed to explain P-wave source spectra for large thrust earthquakes (M_w 5.5 and above). To overcome this, they proposed a double-corner frequency model with a lower-corner frequency associated to source duration and an upper-corner frequency indicating a shorter timescale unrelated to source duration. This upper-corner frequency also exhibits its own scaling relationship. Uchide and Imanishi (2016) reported differences from the omega-square model for smaller earthquakes following the application of a spectral ratio technique to shallow earthquakes with the magnitudes ranging between M_w $3.2 - 4.0$ in Japan. They attributed these differences to fault heterogeneities, applied stress, and high-frequency fall-off exponent variations. We observed high-frequency fall-off parameters ranged from $n = 0.5$ to $n = 3.5$ as they were estimated between 2 and 2.5 aligned more closely with earthquakes with $M_{w-coda} > 3.5$. The smaller magnitudes, on the other hand, exhibited a more scattered pattern in the variation of n (Fig. 5). Eulenfeld and Wegler (2016) argued that a more effective strategy for inverting station displacement spectra to estimate

source parameters involves employing separate estimates of attenuation or accounting for path effects through empirically determined Green's functions. This is, mostly, required for smaller earthquakes (with $n > 2$), given that an omega-square model can distort estimates of f_c and M_0, particularly in the regions of strong frequency-dependent quality factor (Q). Hence, we suggest, when performing inversion for source parameters, it is essential to incorporate independent Q estimates or remove the path influence including the attenuation via empirically determined Green's functions (Eulenfeld and Wegler, 2016).

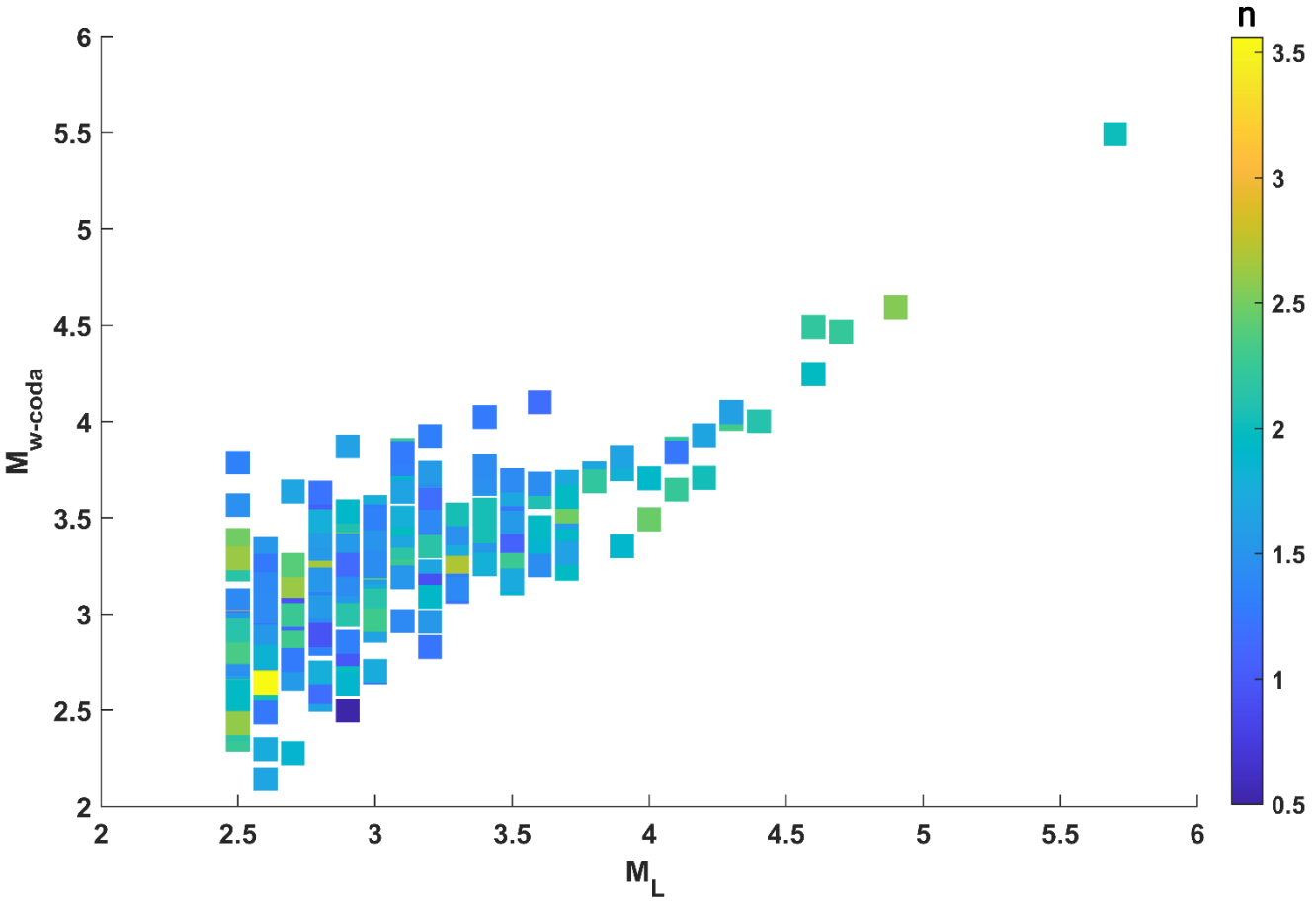

Figure 5: Scatter plot of M_{w-coda} as a function of M_L with high frequency fall-off parameters n. Value of the n, is color coded with legend on the right.

5.3 Coda-derived Moment Magnitude (M_{w-coda})

A comparison between M_L-based catalogue magnitudes (the KOERI earthquake catalogues) and our M_{w-coda} indicates, an overall good accordance between them, except only for a few outliers caused by small-magnitude earthquakes. This can be considered to be an effective usage of a straightforward model using first-order approximation for S-wave scattering with an isotropic acoustic radiative transfer approach in relating the amplitude and decay characteristics of coda wave envelopes to the M_0 of an earthquake at its source.

Here we introduce an empirical equation (Eq. 11) that is obtained based on a linear regression analysis between M_{w-coda} and M_L (Fig. 6). It can be used to convert M_L into M_{w-coda} for local earthquakes in this region conducted a linear regression analysis between M_{w-coda} and M_L (Fig. 6).

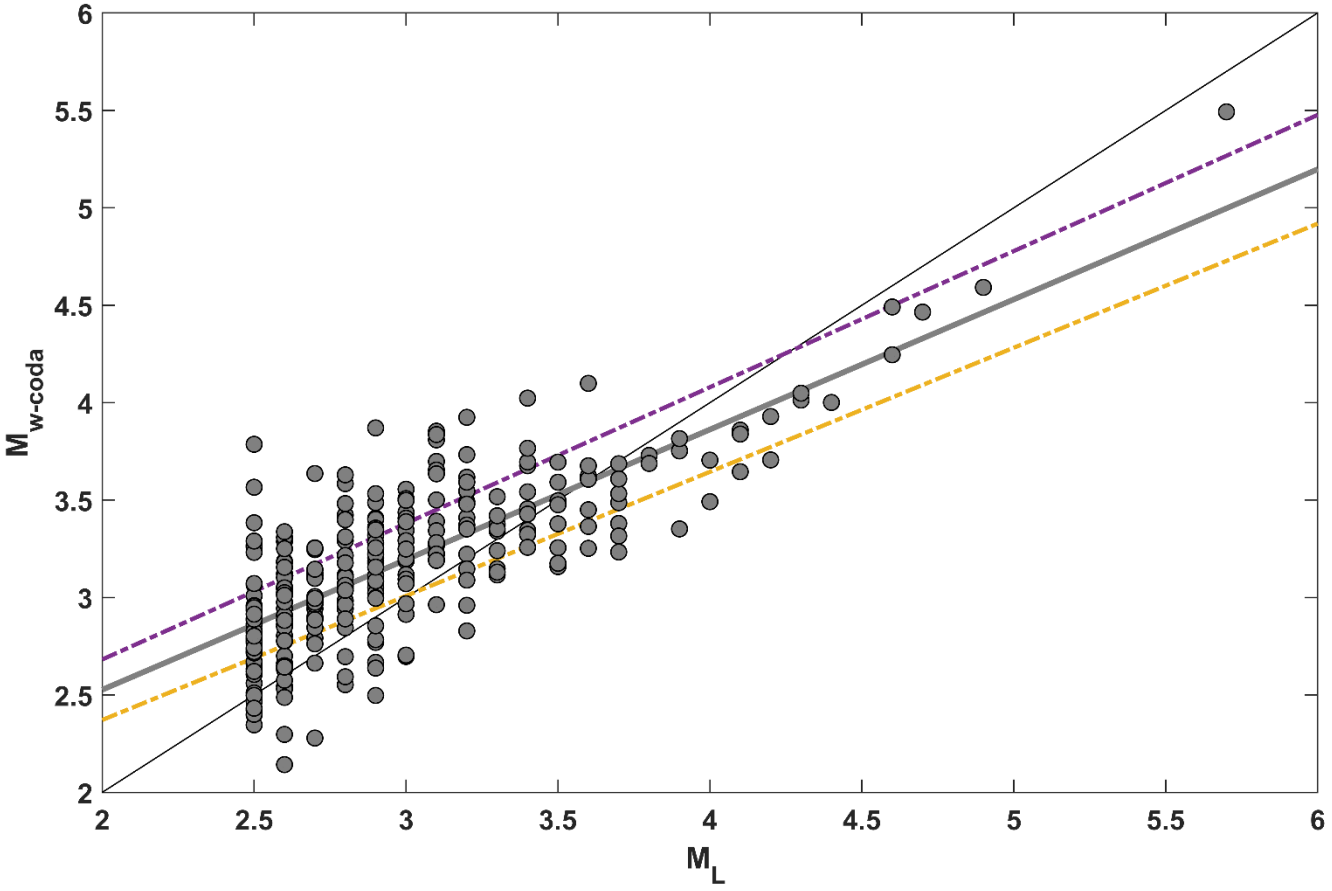

Figure 6: Scatter plot of M_{w-coda} as a function of M_L. Bold grey line represents the linear regression fit and dashed lines are the standard deviation.

$$M_{w-coda} = (0.6677 \mp 0.0309)M_L + 1.1914 \mp 0.09345 \quad (11)$$

In one of the earliest examples of this type of comparison, an empirical linear logarithmic relationship between M_0 and M_L for earthquakes near Oroville, California was established by Bakun and Lindh (1977). Other studies have explored the optimal relation between M_w and M_L using linear and/or nonlinear curve-fitting techniques. Instead of using a single linear fit, Malagnini and Munafò (2018) proposed two separate linear fits for M_L–M_w data points from earthquakes in the central and northern Apennines, Italy, divided by a crossover at $M_L = 4.3$. Various factors i.e., source scaling, crustal attenuation and/or regional attenuation, focal depth, and rigidity of the source region were considered in the regression analyses. Relatively complicated form of empirical functions, for instance, a second-order polynomial form (e.g. Edwards and Rietbrock, 2009) associating local magnitude estimates from the Japan Meteorological Agency (JMA) with the M_w, a hybrid type of scaling

relation (e.g., Goertz-Allmann et al., 2011) with a quadratic form in between ($2 \leq M_L \leq 4$) and linear outside this range tested for Swiss earthquakes, or a quadratic form of correlation between JMA magnitudes and M_w of the seismic activity in the Fukushima Hamadori and northern Ibaraki prefecture areas of Japan (Uchide and Imanishi, 2018) have been proposed in recent years. The empirical curve derived in Uchide and Imanishi (2018) indicated a notable difference between these two magnitude scales. In their work, the graph's slope of 1/2 for microearthquakes was denoted to potential biases stemming from anelastic attenuation and presumable limitations of recording through a finite sampling interval.

Our linear empirical relation between M_{w-coda} and M_L highlight an apparent move-out in Fig. 5 and Eq. 10 as being consistent with findings from early applications of the same type of coda waves modelling studies performed in different geological parts in Türkiye including central and western of the NAFZ (e.g., Gaebler et al., 2019; Izgi et al., 2020) or central Anatolia (Eken, 2019). This likely occurs due to the use of different magnitude scales for comparison. Traditional magnitude scales, such as M_L based on phase amplitude measurements are prone to be affected by attenuation and path variations (Pasyanos et al., 2016). In contrast, seismic-moment-based moment magnitude (M_w) directly measures the strength of an earthquake from fault slip. It is derived from a mostly flat portion of source spectra at lower frequencies, making it less affected by near-surface attenuation. Relatively good agreement between M_{w-coda} and M_L scales for the earthquakes with $M_{w-coda} > 3.5$ demonstrate the efficacy of the nonempirical method in this tectonically complicated region. This is expected for larger earthquakes whose source displacement spectra will carry more energy at lower frequencies. A similar behaviour of such coherence was observed in this region from the previous works where source characteristics of local and regional earthquakes were examined using empirical coda methods assuming simple 1-D radially symmetric path correction (e.g., Eken et al., 2004; Gök et al., 2016). Previous empirical coda envelope modelling studies (e.g., Mayeda et al., 2005a; Morasca et al., 2010) were able to estimate accurate coda-wave-derived source parameters using 2-D path-corrected station techniques that account for amplitude-distance relationships. However, noticeable outliers in our estimates (Fig. 5, 6) for the events with magnitudes less than M_{w-coda} 3.5 could be attributed to potential biases in M_L values extracted from the catalogue as well as small biases in the intrinsic and scattering attenuation terms. Beside this such discrepancies may reflect the effects of mode conversions between body and surface waves or surface-to-surface wave scattering, which extend beyond low frequencies (Sens-Schönfelder and Wegler, 2006).

5.4 Self – Similarity

Accurate estimates of the M_0, overall radiated seismic energy of earthquakes, and associated scaled energy (E_R/M_0) is of great importance for clarifying dynamic modeling scenarios that are helpful to understand ground shaking for large damaging earthquakes as well as the physics behind faulting process. This is mainly because the issue of how big the earthquake ground motions is proportional to radiated energy at the source (e.g., Brune, 1970). Whether earthquakes exhibit self-similar scaling, or larger earthquakes differ in dynamics from smaller ones has been a subject of debate for a long time. Answering this question is essential for both making decent seismic hazard assessment and inferences on the fundamentals of rupture dynamics during an earthquake. Over many years, it has been widely accepted that the E_R/M_0 remains nearly constant for the earthquakes of

varying magnitudes from small-to-large (e.g., Aki, 1967; Kanamori and Anderson, 1975). However, several investigations within the last two decades have observed that this ratio would tend to increase proportionally with the M_0 (e.g., Abercrombie, 1995; Izutani and Kanamori, 2001; Kanamori et al., 1993; Mayeda and Walter, 1996; Mori et al., 2003; Prejean and Ellsworth, 2001; Richardson and Jordan, 2002). Conversely, there exists almost equal number of studies that advocate for a constant energy ratio (e.g., Choy and Boatwright, 1995; Ide et al., 2003; Ide and Beroza, 2001; McGarr, 1999; Prieto et al., 2004). Unfortunately, the substantial uncertainty surrounding seismic energy has led to a diversity of interpretations of this ratio, even among researchers analysing the same dataset.

Recent advancements in scaling the size of earthquake efforts that are based on distinctive approaches using local, regional, and teleseismic data with different frequency contents enable to quantify scalar seismic moments, which usually exhibit small discrepancies (more than a factor of two) for the same given event (Mayeda et al., 2005b). In contrast, the quantity of the released seismic energy of an earthquake is rather a dynamic phenomenon and thus remains a complex endeavour, often resulting in variations exceeding a factor of two among estimates obtained by various techniques (Pérez-Campos et al., 2003). It requires substantial corrections that consider path and site effects across a wide range of frequencies. Further corrections for the directivity and some other heterogeneities in source radiation pattern are equally important and must be concerned. Thus, this ratio has been difficult and becomes the subject of recent debate among experts in the field of seismology. The uncertainty in seismic energy calculations causes different interpretations on the apparent stress associated to the fault rigidity, which may control the energy/moment ratio or seismic energy density. To estimate M_0 and E_R, we benefit from the inherent averaging characteristic of coda waves that has been earlier proved to yield notably less variability in amplitude compared to any conventional direct phase methods (e.g., Eken et al., 2004; Mayeda et al., 2003; Shelly et al., 2022).

The relationship between M_0 and E_R/M_0 observed in this study (Fig. 7) indicates that E_R/M_0 values increase with the M_0 for the crustal earthquakes with M_{w-coda} 2.5 and M_{w-coda} 5.7 implying these earthquakes are likely to follow nonself-similarity. Yoo et al. (2011) previously reported that the E_R/M_0 rapidly increases, in particular, for smaller events ($< M_w \sim$ 3.3). They attributed the size dependency of the scaled energy to the fact that the energy radiation efficiency through seismic waves greatly varying at lower magnitudes. On the other hand, we have not observed any distict change in the trend of E_R/M_0 versus M_0 almost for events in our data. The similar sharp increase has been observed in some early studies of coda-based source modelling, where a different and fully empirical coda normalisation method was used (Mayeda et al., 2007; Morasca et al., 2005; Yoo and Mayeda, 2013). Eulenfeld et al. (2021, 2023) have used the same coda wave modelling approach as used our study, where frequency-dependent source, site, and attenuation properties are inverted in a non-empirical stepwise approach based on a fully analytical RTT assumption in the forward calculation of synthetic coda envelopes. They did also observed deviations from self-similar behaviour of the earthquake rupture. In the previous subsections of the Results and Interpretation, we have already discussed that considering a constant attenuation ratio for events of different sizes, or simply the omega-squared model, may lead to misleading estimates of source properties. As previously stated in Section 5.2, Eulenfeld and Wegler (2016) observed that modelling of source displacement spectra with $n > 2$ under the assumption of the omega-square model ($n = 2$) would still result in a good fit due to the high trade-off between the attenuation and n. However, they observe

that this cause the distortion of f_c and even M_0 estimates if the assumed frequency dependence of Q is not accurately considered. Consequently, they suggest the use of independently obtained estimates of Q when inverting station displacement spectra for source parameters. To reduce this risk, we therefore perform a stepwise inversion scheme where scattering and intrinsic attenuation are also modelled. This allows a realistic consideration of attenuation when estimating the source term at each frequency band. Shearer et al. (2019) have claimed that assuming a fixed fall-off rate, which controls the spectral shape, may artificially result in non-self-similarity. To overcome this, we employed an inversion procedure for modelling source displacement spectra where the n term varied. The inversion for the source displacement spectra, in which independent and more realistic attenuation properties with varying n are considered, leads to a scaling of corner frequencies with M_0 that differs from the scaling associated with self-similarity. Under the assumption of omega-square model a constant E_R/M_0 independent of M_0 (or a constant stress drop independent of magnitude) implying self-similarity corresponds to a proportionality $M_0 \propto f_c^{-3}$. Eulenfeld et al. (2023) noticed that a breaking of self-similarity is not surprising when the exponent defining this trade-off between M_0 and f_c is smaller than -3. It is also equally important to note that the propagation of potential artefacts into the non-constant behaviour of the scaled-energy variation with M_0 can be attributed to the significant impact of the f_c compared to M_0. This is primarily due to the fact that M_0, which is estimated through the low-frequency plateau, is relatively insensitive to the selection of fitting parameters. In contrast, f_c is considerably more sensitive and variable. The most probable artefact, which may be related to the attenuation estimation or spectral fitting process, has the potential to the biased self-similarity analysis. This occurs due to a spurious masking effect associated with excess high-frequency attenuation, which causes the observed shift of fc towards smaller frequencies for smaller events when direct waves are in use (Eulenfeld et al., 2023). The use of Qopen approach, however, provides an advantage of allowing the attenuation to be determined independently from properties of the full waveform envelope instead of the short direct pulse, which diminish possible bias in the estimation of fc. The increasing variation of E_R/M_0 with M_0 resulting from source properties in the present study can be considered reliable, given that the Qopen algorithm is less sensitive to potential artefacts. This is due to the advantages of using coda waves and implementing a more realistic knowledge of frequency-dependent attenuation during modelling for source displacement spectra. Finally our initial observation on the variation of scaled energy implies that different rupture dynamics works for large earthquakes than small ones and the seismic energy radiates more efficiently for relatively large earthquakes in the Sea of Marmara located at the north-western part of the NAFZ.

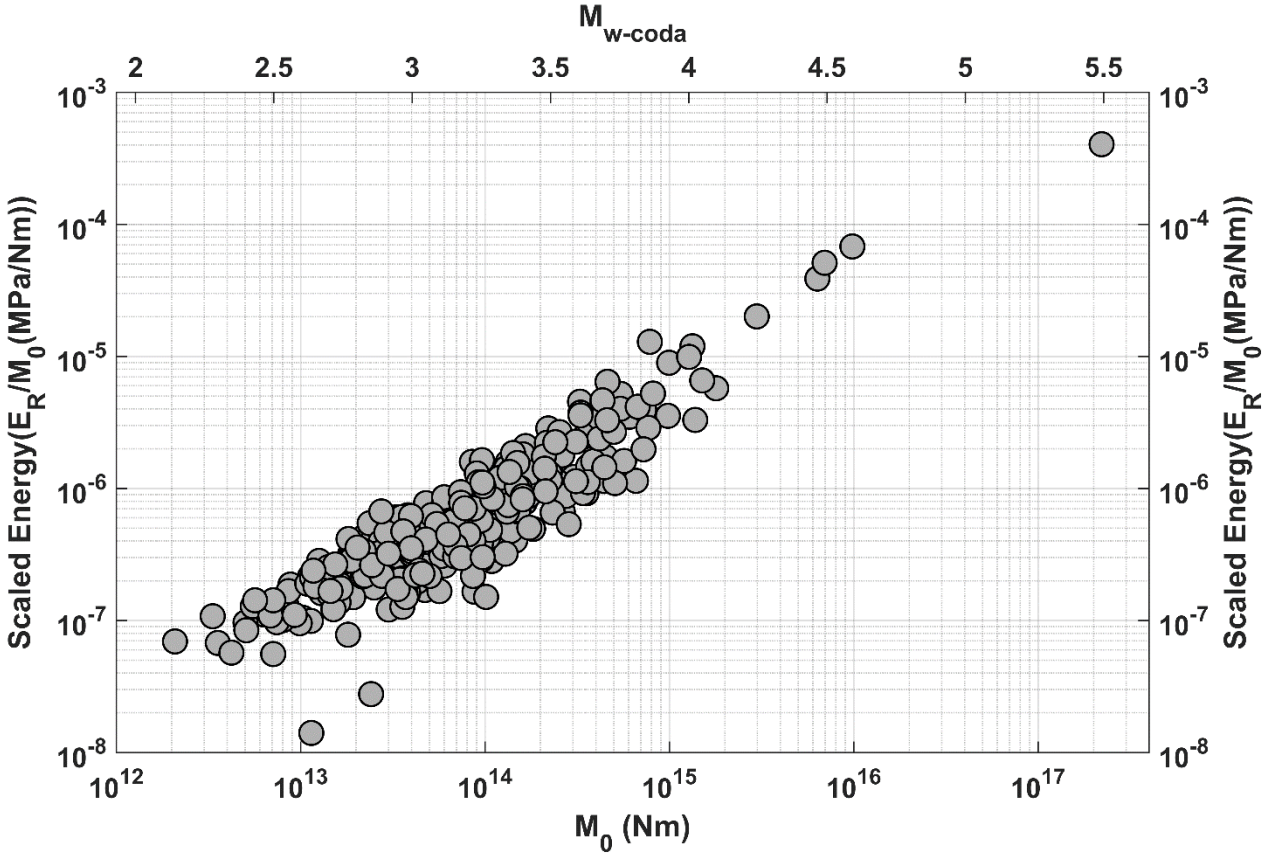

Figure 7: Scatter plot of scaled energy (E_R/M_0) as a function of both M_0 and M_w.

6 Conclusion

This study provides the physical measure of the released seismic energy in M_{w-coda} for minor to moderate size local earthquakes ($2.5 \leq M_w \leq 5.7$) that occurred between 2018 and 2020 in the Sea of Marmara Region, NW Türkiye. This was accomplished by using digital waveform recordings taken from 49 three-component broadband seismic stations located within the study region. We used Radiative Transfer Theory for the forward calculation of synthetic coda wave envelopes during an iterative inversion procedure employing a stepwise manner to model the source properties as well as site, path effects simultaneously based on the smallest misfit between observed and synthetic envelopes. The good accordance between M_{w-coda} and M_L proves the competence of this non-empirical coda wave approach to obtain reliable estimates of source properties in this complex tectonic setting. The variability of the high-frequency fall-off parameter highlighted that for smaller earthquakes ($n > 2$), considering an omega-square model could distort estimates of f_c and M_0. This effect is particularly pronounced in regions where Q exhibits strong frequency dependency. A linear regression analysis further provided an

empirical relation developed between M_{w-coda} and M_L, which can be a useful tool in the future to quickly convert catalog magnitudes into M_w for local earthquakes in the study area. Finally, the scaled energy (E_R/M_0) exhibits an increasing pattern with reliable coda wave-derived seismic moment estimates at almost all magnitude ranges as this implies small-to-moderate size seismic activity in the region indicates a nonself-similar scaling at their source.

Code Availability

The Python code (Qopen) utilized for performing inverse modelling is accessible under the permissive MIT license. It can be obtained from https://github.com/trichter/qopen (last accessed on 28 July 2024) and is cited as Eulenfeld (2020) (https://doi.org/10.5281/zenodo.3953654).

Data Availability

Digital waveform recordings of local earthquakes analysed in the present study and station metadata were acquired from the seismological data management facilities of the Kandilli Observatory and Earthquake Research Institute (KOERI).

Author Contribution

The paper was initially prepared by BO and TE. PG provided a comprehensive review of the manuscript, especially the Methods section. TT contributed to both the writing of the paper and the interpretation of the results, as well as providing insights into the tectonic background."

Competing Interests

The contact author has declared that none of the authors has any competing interests.

Acknowledgement

This study is a part of an ongoing Ph.D. thesis by Berkan Özkan under the supervision of Assoc. Prof. Dr. Tuna Eken. Berkan Özkan, Tuna Eken, and Tuncay Taymaz, would like to thank Istanbul Technical University, the National Scientific and Technological Research Council of Türkiye (TÜBİTAK), and the Alexander von Humboldt Foundation for further providing computing facilities through Humboldt-Stiftung Follow-Up Programme. The authors would like to express their gratitude to Tom Eulenfeld for his valuable contributions to the discussion on self-similarity.. We express our sincere appreciation to Editor CharLotte Krawczyk, Topic Editor Simone Pilia, Gizem Izgi, and one anonymous reviewer for their invaluable efforts, which substantially contributed to the refinement of this article.

References

Abercrombie, R. E.: Earthquake source scaling relationships from -1 to 5 ML using seismograms recorded at 2.5-km depth. J. Geophys. Res., 100(B12), 24015–24036, doi:10.1029/95jb02397, 1995.

Aki, K.: Scaling law of seismic spectrum. J. Geophys. Res., 72(4), 1217–1231, doi:10.1029/JZ072I004P01217, 1967.

Aki, K.: Analysis of The Seismic Coda of Local Earthquakes as Scattered Waves. J. Geophys. Res., 74(2), 615–631, doi:10.1029/jb074i002p00615, 1969.

Aki, K. and Chouet, B.: Origin of coda waves: Source, attenuation and scattering effects. J. Geophys. Res., 80(23), 3322–3342, doi:10.1029/JB080i023p03322, 1975.

Ambeh, W. B. and Fairhead, J. D.: Spectral characteristics and source parameters of microearthquakes from the Mt Cameroon volcanic region, West Africa. Geophys. J. Int., 106(1), 229–237, doi:10.1111/J.1365-246X.1991.TB04613.X, 1991.

Ambraseys, N. N. and Jackson, J. A.: Seismicity of the Sea of Marmara (Turkey) since 1500. Geophys. J. Int., 141(3), F1–F6, doi:10.1046/j.1365-246x.2000.00137.x, 2000.

Atkinson, G. M.: A Comparison of Eastern North American Ground Motion Observations with Theoretical Predictions. Seismol. Res. Lett., 61(3–4), 171–180, doi:10.1785/GSSRL.61.3-4.171, 1990.

Bakun, W. H. and Lindh, A. G.: Local magnitudes, seismic moments and coda durations for earthquakes near Oroville, California. Bull. Seism. Soc. Am., 67(3), 615–629, doi:10.1785/BSSA0670030615, 1977.

Barka, A., Akyüz, H. S., Altunel, E., Sunal, G., Çakir, Z., Dikbas, A., Yerli, B., Armijo, R., Meyer, B., de Chabalier, J. B., Rockwell, T., Dolan, J. R., Hartleb, R., Dawson, T., Christofferson, S., Tucker, A., Fumal, T., Langridge, R., Stenner, H., … Page, W.: The Surface Rupture and Slip Distribution of the 17 August 1999 İzmit Earthquake (M 7.4), North Anatolian Fault. Bull. Seism. Soc. Am., 92(1), 43–60, doi:10.1785/0120000841, 2002.

Boatwright, J. and Fletcher, J. B.: The partition of radiated energy between P and S waves. Bull. Seism. Soc. Am., 74(2), 361–376, doi:10.1785/BSSA0740020361, 1984.

Bohnhoff, M., Bulut, F., Dresen, G., Malin, P. E., Eken, T. and Aktar, M.: An earthquake gap south of Istanbul. Nat. Commun., 4(1), 1999, doi:10.1038/ncomms2999, 2013.

Bohnhoff, M., Martínez-Garzón, P., Bulut, F., Stierle, E. and Ben-Zion, Y.: Maximum earthquake magnitudes along different sections of the North Anatolian fault zone. Tectonophysics, 674, 147–165, doi:10.1016/j.tecto.2016.02.028, 2016.

Brune, J. N.: Tectonic stress and the spectra of seismic shear waves from earthquakes J. Geophys. Res., 75(26), 4997–5009, doi:10.1029/JB075I026P04997, 1970.

Choy, G. L. and Boatwright, J. L.: Global patterns of radiated seismic energy and apparent stress. J. Geophys. Res., 100(B9), doi:10.1029/95JB01969, 1995.

Denolle, M. A. and Shearer, P. M.: New perspectives on self-similarity for shallow thrust earthquakes. J. Geophys. Res. Solid Earth, 121(9), 6533–6565, doi:10.1002/2016JB013105, 2016.

Durand, V., Bouchon, M., Karabulut, H., Marsan, D., Schmittbuhl, J., Durand, V., Bouchon, M., Karabulut, H., Marsan, D. and Schmittbuhl, J.: Link between Coulomb stress changes and seismic activation in the eastern Marmara Sea after the 1999, Izmit (Turkey), earthquake. J. Geophys. Res. Solid Earth, 118(2), 681–688, doi:10.1002/JGRB.50077, 2013.

Edwards, B. and Rietbrock, A.: A comparative study on attenuation and source-scaling relations in the Kantō, Tokai and Chubu regions of Japan, using data from Hi-net and KiK-net. Bull. Seism. Soc. Am., 99(4), 2435–2460, doi:10.1785/0120080292, 2009.

Eken, T., Mayeda, K., Hofstetter, A., Gök, R., Örgülü, G. and Turkelli, N.: An application of the coda methodology for moment-rate spectra using broadband stations in Turkey. Geophys. Res. Let., 31(11), doi:10.1029/2004GL019627, 2004.

Eken, T.: Moment magnitude estimates for central Anatolian earthquakes using coda waves. Solid Earth, 10(3), 713–723, doi:10.5194/se-10-713-2019, 2019.

Ergintav, S., Reilinger, R. E., Çakmak, R., Floyd, M., Cakir, Z., Doğan, U., King, R. W., McClusky, S. and Özener, H.: Istanbul's earthquake hot spots: Geodetic constraints on strain accumulation along faults in the Marmara seismic gap. Geophys. Res. Let., 41(16), 5783–5788, doi:10.1002/2014GL060985, 2014.

Eulenfeld, T. and Wegler, U.: Measurement of intrinsic and scattering attenuation of shear waves in two sedimentary basins and comparison to crystalline sites in Germany. Geophys. J. Int., 205(2), 744–757, doi:10.1093/gji/ggw035, 2016.

Eulenfeld, T. and Wegler, U.: Crustal intrinsic and scattering attenuation of high-frequency shear waves in the contiguous United States. J. Geophys. Res. Solid Earth, 122, 4676–4690, doi: 10.1002/2017JB014038, 2017.

Eulenfeld, T.: Toward Source Region Tomography with Intersource Interferometry: Shear Wave Velocity From 2018 West Bohemia Swarm Earthquakes. J. Geophys. Res. Solid Earth, 125, doi:10.1029/2020JB019931, 2020.

Eulenfeld T., Dahm T., Heimann S., and Wegler U.: Fast and robust earthquake source spectra and moment magnitudes from envelope inversion, Bull. Seism. Soc. Am., doi:10.1785/0120210200, 2021.

Eulenfeld, T., Hillers, G., Vuorinen, T. A., and Wegler, U.: Induced earthquake source parameters, attenuation, and site effects from waveform envelopes in the fennoscandian shield. J. Geophys. Res. Solid Earth, 128(4), doi:10.1029/2022jb025162, 2023.

Favreau, P. and Archuleta, R. J.: Direct seismic energy modelling and application to the 1979 Imperial Valley earthquake. Geophys. Res. Let., 30(5), doi:10.1029/2002gl015968, 2003.

Gaebler, P. J., Eulenfeld, T. and Wegler, U.: Seismic scattering and absorption parameters in the W-Bohemia/Vogtland region from elastic and acoustic radiative transfer theory. Geophys. J. Int., 203(3), 1471–1481, doi:10.1093/gji/ggv393, 2015a.

Gaebler, P. J., Sens-Schönfelder, C. and Korn, M.: The influence of crustal scattering on translational and rotational motions in regional and teleseismic coda waves. Geophys. J. Int., 201(1), 355–371, doi:10.1093/GJI/GGV006, 2015b.

Gaebler, P., Eken, T., Bektaş, H. Ö., Eulenfeld, T., Wegler, U. and Taymaz, T.: Imaging of shear wave attenuation along the central part of the North Anatolian Fault Zone, Turkey. J. Seismol., 23(4), 913–927, doi:10.1007/S10950-019-09842-1, 2019.

Goertz-Allmann, B. P., Goertz, A. and Wiemer, S.: Stress drop variations of induced earthquakes at the Basel geothermal site. Geophys. Res. Let., 38(9), doi:10.1029/2011gl047498, 2011.

Gök, R., Hutchings, L., Mayeda, K. and Kalafat, D.: Source parameters for 1999 North Anatolian fault zone aftershocks. Pure Appl. Geophys, 166(4), 547–566, doi:10.1007/s00024-009-0461-x, 2009.

Gök, R., Kaviani, A., Matzel, E. M., Pasyanos, M. E., Mayeda, K., Yetirmishli, G., El Hussain, I., Al Amri, A., Al Jeri, F., Godoladze, T., Kalafat, D., Sandvol, E. A. and Walter, W. R.: Moment magnitudes of local/regional events from 1D coda calibrations in the broader middle east region. Bull. Seism. Soc. Am., 106(5), 1926–1938, doi:10.1785/0120160045, 2016.

Gusev, A. and Abubakirov, I: Simulated envelopes of non-isotropically scattered body waves as compared to observed ones: Another manifestation of fractal heterogeneity. Geophys. J. Int., 127, 49–60, doi:10.1111/j.1365-246X.1996.tb01534.x, 1996.

Hanks, T. C. and Kanamori, H.: A moment magnitude scale. Geophys. Res. B Solid Earth, 84(B5), 2348–2350, doi:10.1029/JB084iB05p02348, 1979.

Ide, S. and Beroza, G. C: Does apparent stress vary with earthquake size? Geophys. Res. Let., 28(17), 3349–3352, doi:10.1029/2001GL013106, 2001.

Ide, S., Beroza, G. C., Prejean, S. G. and Ellsworth, W. L.: Apparent break in earthquake scaling due to path and site effects on deep borehole recordings. J. Geophys. Res. Solid Earth., 108(B5), 2271, doi:10.1029/2001JB001617, 2003.

Irmak, T.S., Yolsal-Çevikbilen, S., Eken, T., Doğan, B., Erman, C., Yavuz, E., Alçık, H., Gaebler, P., Pınar, A., Taymaz, T.: Source Characteristics and Seismotectonic Implications of 26 September 2019 Silivri (High)-Kumburgaz Basin Earthquake (Mw 5.7) and Evaluation of its Aftershocks at the North Anatolian Fault Zone (Central Marmara Sea, NW Turkey), Geophys. J. Int., Volume 227, Issue 1, October 2021, Pages 383–402, doi:10.1093/gji/ggab233, 2021.

Izgi, G., Eken, T., Gaebler, P., Eulenfeld, T. and Tuncay, T.: Crustal seismic attenuation parameters in the western region of the North Anatolian Fault Zone. J. Geodynam., 134, 101694, doi:10.1016/j.jog.2020.101694, 2020.

Izutani, Y. and Kanamori, H.: Scale-dependence of seismic energy-to-moment ratio for strike-slip earthquakes in Japan. Geophys. Res. Let., 28(20), 4007–4010, doi:10.1029/2001GL013402, 2001.

Joyner, W. B.: A scaling law for the spectra of large earthquakes. Bull. Seism. Soc. Am., 74(4), 1167–1188, doi:10.1785/BSSA0740041167, 1984.

Kanamori, H. and Anderson, D. L.: Theoretical basis of some empirical relations in seismology. Bull. Seism. Soc. Am., 65(5), 1073–1095, doi:10.1785/BSSA0650051073, 1975.

Kanamori, H., Ekström, G., Dziewonski, A., Barker, J. S. and Sipkin, S. A.: Seismic radiation by magma injection: An anomalous seismic event near Tori Shima, Japan. J. Geophys. Res. Solid Earth, 98(B4), 6511–6522, doi:10.1029/92JB02867, 1993.

King, G. C. P., Hubert-Ferrari, A., Nalbant, S. S., Meyer, B., Armijo, R. and Bowman, D.: Coulomb interactions and the 17 August 1999 Izmit, Turkey earthquake. C. R. Acad. Sci.-Ser. IIA-Earth Planet. Sci., 333(9), 557–569, doi:10.1016/S1251-8050(01)01676-7, 2001.

Kwiatek, G., Plenkers, K. and Dresen, G.: Source parameters of picoseismicity recorded at Mponeng deep gold mine, South Africa: Implications for scaling relations. Bull. Seism. Soc. Am., 101(6), 2592–2608, doi:10.1785/0120110094, 2011.

Malagnini, L., Mayeda, K., Akinci, A. and Bragato, P. L.: Estimating Absolute Site Effects. Bull. Seism. Soc. Am., 94(4), 1343–1352, doi:10.1785/012003161, 2004.

Malagnini, L. and Munafò, I.: On the relationship between ML and MW in a broad range: An example from the Apennines, Italy. Bull. Seism. Soc. Am., 108(2), 1018–1024, doi:10.1785/0120170303, 2018.

Martínez-Garzón, P., Bohnhoff, M., Mencin, D., Kwiatek, G., Dresen, G., Hodgkinson, K., Nurlu, M., Kadirioglu, F. T., & Kartal, R. F.: Slow strain release along the Eastern Marmara Region Offshore Istanbul in conjunction with enhanced local seismic moment release. Earth and Planetary Sci. Let., 510, 209–218, doi:10.1016/j.epsl.2019.01.001, 2019

Martínez-Garzón, P., Durand, V., Bentz, S., Kwiatek, G., Dresen, G., Turkmen, T., Nurlu, M., & Bohnhoff, M.: Near-fault monitoring reveals combined seismic and slow activation of a fault branch within the Istanbul–Marmara seismic gap in northwest Turkey Seism. Res. Let., 92(6), 3743–3756, doi:10.1785/0220210047, 2021.

Mayeda, K. and Walter, W. R.: Moment, energy, stress drop and source spectra of western United States earthquakes from regional coda envelopes. J. Geophys. Res. Solid Earth, 101(5), 11195–11208, doi:10.1029/96jb00112, 1996.

Mayeda, K., Hofstetter, A., O'Boyle, J. L. and Walter, W. R.: Stable and transportable regional magnitudes based on coda-derived moment-rate spectra. Bull. Seism. Soc. Am., 93(1), 224–239, doi:10.1785/0120020020, 2003.

Mayeda, K., Malagnini, L., Phillips, W. S., Walter, W. R. and Dreger, D.: 2-D or not 2-D, that is the question: A northern California test. Geophys. Res. Let., 32(12), 1–5, doi:10.1029/2005GL022882, 2005a.

Mayeda, K., Gök, R., Walter, W. R. and Hofstetter, A.: Evidence for non-constant energy/moment scaling from coda-derived source spectra. Geophys. Res. Let., 32(10), 1–4, doi:10.1029/2005GL022405, 2005b.

Mayeda, K., L. Malagnini, and W. R. Walter: A new spectral ratio method using narrow band coda envelopes: Evidence for non-self-similarity in the Hector Mine sequence, Geophys. Res. Lett., 34, L11303, doi:10.1029/2007GL03004, 2007.

McGarr, A.: On relating apparent stress to the stress causing earthquake fault slip. J. Geophys. Res. Solid Earth, 104(B2), 3003–3011, doi:10.1029/1998JB900083, 1999.

Morasca, P., Mayeda, K., Gök, R., Phillips, W. and Malagnini, L.: 2D Coda and Direct-Wave Attenuation Tomography in Northern Italy. Bull. Seism. Soc. Am., 98, 1936–1946, doi:10.1785/0120070089, 2008.

Morasca, P., Massa, M., Laprocina, E., Mayeda, K., Phillips, S., Malagnini, L., Spallarossa, D., Costa, G. and Augliera, P.: Improved 2-D attenuation analysis for Northern Italy using a merged dataset from selected regional seismic networks. J. Seismol., 14(4), 727–738, doi:10.1007/s10950-010-9194-7, 2010.

Mori, J., Abercrombie, R. E. and Kanamori, H.: Stress drops and radiated energies of aftershocks of the 1994 Northridge, California, earthquake. J. Geophys. Res. Solid Earth, 108(B11), 2545, doi:10.1029/2001JB000474, 2003.

Paasschens, J.: Solution of the time-dependent Boltzmann equation. Physical Review E - Statistical Physics, Plasmas, Fluids and Related Interdisciplinary Topics, 56(1), 1135–1141, doi:10.1103/PhysRevE.56.1135, 1997.

Papageorgiou, A, S. and Aki, K.: A specific barrier model for the quantitative description of inhomogeneous faulting and the prediction of strong ground motion. I. Description of the model. Bull. Seism. Soc. Am., 73 (3): 693–722, doi:10.1785/BSSA0730030693, 1983.

Pasyanos, M. E., Gök, R. and Walter, W. R.: 2D variations in coda amplitudes in the middle east. Bull. Seism. Soc. Am., 106(5), 1915–1925, doi:10.1785/0120150336, 2016.

Patton, H. J. and Walter, W. R.: Regional moment magnitude relations for earthquakes and explosions. Geophys. Res. Let., 20(4), 277–280, doi:10.1029/93GL00298, 1993.

Pérez-Campos, X., Singh, S. K. and Beroza, G. C.: Reconciling Teleseismic and Regional Estimates of Seismic Energy. Bull. Seism. Soc. Am., 93(5), 2123–2130, doi:10.1785/0120020212, 2003.

Prejean, S. G. and Ellsworth, W. L.: Observations of Earthquake Source Parameters at 2 km Depth in the Long Valley Caldera, Eastern California. Bull. Seism. Soc. Am., 91(2), 165–177, doi:10.1785/0120000079, 2001.

Prieto, G. A., Shearer, P. M., Vernon, F. L. and Kilb, D.: Earthquake source scaling and self-similarity estimation from stacking P and S spectra. J. Geophys. Res. Solid Earth, 109(B8), doi:10.1029/2004JB003084, 2004.

Przybilla, J. and Korn, M.: Monte Carlo simulation of radiative energy transfer in continuous elastic random media—three-component envelopes and numerical validation. Geophys. J. Int., 173, 566–576, doi:10.1111/j.1365-246X.2008.03747.x, 2008.

Rautian, T. G. and Khalturin, V. I.: The use of the coda for determination of the earthquake source spectrum. Bull. Seism. Soc. Am., 68(4), 923–948, doi:10.1785/BSSA0680040923, 1978.

Richardson, E. and Jordan, T. H.: Seismicity in deep gold mines of South Africa: Implications for tectonic earthquakes. Bull. Seism. Soc. Am., 92(5), 1766–1782, doi:10.1785/0120000226, 2002.

Ryzhik, L., Papanicolaou, G. and Keller, J. B.: Transport equations for elastic and other waves in random media. Wave Motion, 24(4), 327–370, doi:10.1016/S0165-2125(96)00021-2, 1996.

Sato, T., Kasahara, J., Taymaz, T., Ito, M., Kamimura, A., Hayakawa, T. and Tan, O.: A study of microearthquake seismicity and focal mechanisms within the Sea of Marmara (NW Turkey) using ocean bottom seismometers (OBSs). Tectonophysics, 391(1), 303–314, doi:10.1016/j.tecto.2004.07.018, 2004.

Sato, H., Fehler, M. and Maeda, T.: Seismic Wave Propagation and Scattering in the Heterogeneous Earth: Second Edition. In Seismic Wave Propagation and Scattering in the Heterogeneous Earth: Second Edition, doi:10.1007/978-3-642-23029-5, 2012.

Schmittbuhl, J., Karabulut, H., Lengliné, O. and Bouchon, M.: Long-lasting seismic repeaters in the Central Basin of the Main Marmara Fault. Geophys. Res. Let., 43(18), 9527–9534, doi:10.1002/2016GL070505, 2016.

Sens-Schönfelder, C. and Wegler, U.: Radiative transfer theory for estimation of the seismic moment. Geophys. J. Int, 167(3), 1363–1372, doi:10.1111/j.1365-246X.2006.03139.x, 2006.

Shelly, D. R., Mayeda, K., Barno, J., Whidden, K. M., Moschetti, M. P., Llenos, A. L., Rubinstein, J. L., Yeck, W. L., Earle, P. S., Gök, R. and Walter, W. R.: A Big Problem for Small Earthquakes: Benchmarking Routine Magnitudes and Conversion Relationships with Coda Envelope-Derived Mw in Southern Kansas and Northern Oklahoma. Bull. Seism. Soc. Am., 112(1), 210–225, doi:10.1785/0120210115, 2022.

Shearer, P. M., Abercrombie, R. E., Trugman, D. T., and Wang, W.: Comparing EGF methods for estimating corner frequency and stress drop from p wave spectra. J. Geophys. Res.: Solid Earth, 124(4), 3966–3986, doi:10.1029/2018jb016957, 2019

Stein, R. S., Barka, A. A. and Dieterich, J. H.: Progressive failure on the North Anatolian Fault since 1939 by earthquake stress triggering. Geophys. J. Int, 128(3), 594–604, doi:10.1111/j.1365-246x.1997.tb05321.x , 1997.

Taymaz, T., Jackson, J.A. and McKenzie, D.: Active Tectonics of the North and Central Aegean Sea. Geophys. J. Int., 106, 433-490, doi: 10.1111/j.1365-246X.1991.tb03906.x, 1991.

Taymaz, T., Westaway, R. and Reilinger, R.: Active faulting and crustal deformation in the Eastern Mediterranean region. Tectonophysics, 391(1), 1–9, doi:10.1016/j.tecto.2004.07.005, 2004.

Taymaz, T., Yılmaz, Y. and Dilek, Y.: The Geodynamics of the Aegean and Anatolia: Introduction. In: The Geodynamics of the Aegean and Anatolia (eds. Tuncay Taymaz, Yücel Yılmaz and Yıldırım Dilek), pp. 1-16, The Geological Society of London, Special Publications Book, Vol: 291, ISBN: 978-1-86239-239-7, 2007.

Taymaz, T., Ganas, A., Yolsal-Çevikbilen, S., Vera, F., Eken, T., Erman, C., Keleş, D., Kapetanidis, V., Valkaniotis, S., Karasante, I., Tsironi, V., Gaebler, P., Melgar, D. and Öcalan, T.: Source mechanism and rupture process of the 24 January 2020 MW 6.7 Doğanyol–sivrice earthquake obtained from seismological waveform analysis and space geodetic observations on the East Anatolian Fault Zone (Turkey). Tectonophysics, 804, 228745, doi:10.1016/j.tecto.2021.228745, 2021.

Uchide, T. and Imanishi, K.: Small earthquakes deviate from the omega-square model as revealed by multiple spectral ratio analysis. Bull. Seism. Soc. Am., 106(3), 1357–1363, doi:10.1785/0120150322, 2016.

Uchide, T. and Imanishi, K.: Underestimation of Microearthquake Size by the Magnitude Scale of the Japan Meteorological Agency: Influence on Earthquake Statistics. J. Geophys. Res. Solid Earth, 123(1), 606–620, doi:10.1002/2017JB014697, 2018.

Walter, W. R., Mayeda, K. M. and Patton, H. J.: Phase and spectral ratio discrimination between NTS earthquakes and explosions. Part I: Empirical observations. Bull. Seism. Soc. Am., 85(4), 1050–1067, doi:10.1785/BSSA0850041050, 1995.

Wollin, C., Bohnhoff, M., Martínez-Garzón, P., Küperkoch, L. and Raub, C.: A unified earthquake catalogue for the Sea of Marmara Region, Turkey, based on automatized phase picking and travel-time inversion: Seismotectonic implications. Tectonophysics, 747–748, 416–444, doi:10.1016/j.tecto.2018.05.020, 2018.

Yoo, S. H., Rhie, J., Choi, H. and Mayeda, K.: Coda-derived source parameters of earthquakes and their scaling relationships in the Korean peninsula. Bull. Seism. Soc. Am., 101(5), 2388–2398, doi:10.1785/0120100318, 2011.

Yoo, S. H., and Mayeda, K.: Validation of non-self-similar source scaling using ground motions from the 2008 Wells, Nevada, earthquake sequence. Bull. Seism. Soc. Am., 103(4), 2508–2519, doi:10.1785/0120120327, 2013.

Zeng, Y., Su, F. and Aki, K.: Scattering wave energy propagation in a random isotropic scattering medium: 1. Theory. J. Geophys. Res., 96, 607–619, doi:10.1029/90JB02012, 1991.